Journal of Materials Science: Materials in Electronics (2019) 30:16659–16665
https://doi.org/10.1007/s10854-019-02046-w

The bipolar resistive switching and negative differential resistance of NiO films induced by the interface states

Pan Yang[1] · Wei Peng[1] · Lingxia Li[1] · Shihui Yu[1] · Haoran Zheng[1]

Received: 7 June 2019 / Accepted: 13 August 2019 / Published online: 20 August 2019
© Springer Science+Business Media, LLC, part of Springer Nature 2019

Abstract

The Au/NiO/Pt structure was fabricated by magnetron sputtering on the $TiO_x/SiO_2/Si$ substrates to investigate the bipolar resistive switching and negative differential resistance in details. The XRD results shows the NiO films have the (111) preferential orientation. XPS measurements shows the Ni^{3+} exists in NiO films, indicating that the p-type nonstoichiometric nickel oxide films forms. The I–V characteristic curves show that the bipolar resistive switching and negative differential resistance seriously depend on the scan mode of applied voltage. When the applied voltage scans from negative voltage to positive voltage and return to negative voltage, the negative differential resistance is obtained accompanied with the distinct resistive switching characteristic. However, the negative differential resistance characteristic disappears when the applied voltage swept from 0 V to positive voltage and returned to 0 V from negative voltage. This behavior is highly affected by the interface states, located at the interface of Au and p-NiO films, trap and release the holes. The schematic diagram of energy band structure and interface state can clearly depict the trap-and-release process, resulting the bipolar resistive switching accompanied with the negative differential resistance.

1 Introduction

Resistive switching (RS) effect with the metal/oxide/metal structures has drawn enormous attention due to the device's low power consumption, rapid switching response, simple cell structure, and CMOS technology compatibility [1, 2]. The excellent character makes it a prominent candidate for next generation nonvolatile memory [3, 4]. The resistive switching phenomenon with the low-resistance state and high-resistance state has been investigated in many materials, such as binary oxides (NiO [4, 5], TiO_2 [6–8], SiO_2 [9], Cr_2O_3 [10] and ZnO [11]) and perovskite oxides ($SrTiO_3$ [12] and $NiFe_2O_4$ [13]). Various mechanisms are proposed to understand the phenomena. The contribution of formation and dissolution of conductive filaments to the RS has been investigated widely [14–18]. And the conductive filaments are confirmed by direct observation with transmission electron microscopy (TEM) [4, 19] and conducting atomic force microscopy (CAFM) [20]. Nevertheless, the rectification characteristic observed in NiO films [21, 22], ZnO films [23] and $BaTiO_3$ [24] films indicates the conductive filaments cannot explain it well. The modification of depletion layer width near interface controlled by the external voltage bias is often used to understand the bipolar RS effect in Schottky junction, but it is difficult to explain the negative differential resistance (NDR) though the rectification characteristic can be explained [25]. The NDR is also reported in TiO_2 and $Gd_{0.5}Sr_{0.5}MnO_3$ induced by Joule-heating [6, 26]. The current-controlled NDR also is out of operation to the voltage-controlled NDR. Thus, the phenomenon, resistive switching accompanied with the NDR, needs to be further studied to have a better understand on the resistive switching.

Among the various oxide films exhibiting resistive switching characteristic, the NiO has drawn enormous researchers' attention due to the simple constituents and high on/off ratio [27]. In this paper, the NiO films were deposited by RF magnetron sputtering with the Au/NiO/Pt structure to investigated the resistive switching accompanied with the NDR. For understanding this phenomenon profoundly, the current–voltage curves were measured with three scanning modes: (1) the applied voltage swept from negative voltage

✉ Lingxia Li
lingxiali66@163.com

✉ Shihui Yu
ysh728@126.com

[1] School of Microelectronics and Key Laboratory for Advanced Ceramics and Machining Technology, Tianjin University, Tianjin 300072, People's Republic of China

to positive voltage and returned to negative voltage with DC bias performed by Keithley 4200 (mode I), (2) the applied voltage swept from negative voltage to positive voltage and returned to negative voltage under different scanning rate with the fixed voltage step 0.5 V performed by Radiant Precision LC (mode II) and (3) the applied voltage swept from positive voltage to negative voltage and returned to positive voltage with different frequency performed by Radiant Precision LC (mode III).

2 Experimental procedures

The device with the Au/NiO/Pt structure was fabricated by magnetron sputtering. The bottom electrodes Pt were deposited on $TiO_x/SiO_2/Si$ substrate by DC magnetron sputtering. The NiO films with 550 nm were deposited by RF magnetron sputtering. The solid-state reaction method was adopted to prepare the NiO target. Appropriate amount polyvinyl alcohol organic binder was added into the NiO powder. After that, the mixture was ball-milled for 12 h using deionized water as medium and then pressed into a disk with 6 cm diameter. The target disk was sintered at 1200 °C for 5 h in air. A distance of 10 cm was maintained between target and substrate. Before sputtering, the vacuum chamber was evacuated down to 5×10^{-5} Torr. The total pressure of the sputtering ambient was fixed at 12 mTorr. The ratio of O_2/Ar was keep at 1/14 by using high purity argon (Ar) and oxygen (O_2). The radio frequency power was maintained at 135 W. After the deposition, NiO thin films were treated for 10 min in air at 200 °C. The top electrodes Au with 200 µm diameter were sputtered through a mask. The Alpha Step D-100 profilometer (KLA-Tencor, California, USA) was used to determine the thickness of NiO thin films. The phase composition and valence state information were characterized by X-ray diffractometer (Rigaku D/MAX-2500, Akishima, Tokyo, Japan) with Cu Kα radiation (λ = 0.154 nm) and X-ray photoelectron spectroscopy (XPS, Kratos AXIS Ultra DLD, Japan). The I–V characteristic were performed by Keithley 4200 and Radiant Precision LC.

3 Results and discussion

Figure 1a shows the device structure with top Au electrode (0.2 mm in diameter). The voltage is applied to the top Au electrode and the bottom Pt electrode is contact to ground. The characteristic diffraction peaks of NiO films are shown in Fig. 1b, which are comparable to those of the powder diffraction pattern in JCPDS card no. 89-7130. The peak at 38.28° is assigned to the TiO_2 and peaks at 44.52° and 64.86° are assigned to the SiO_2, which originate from the $TiO_x/SiO_2/Si$ substrate. The peak at 69.79° is induced by

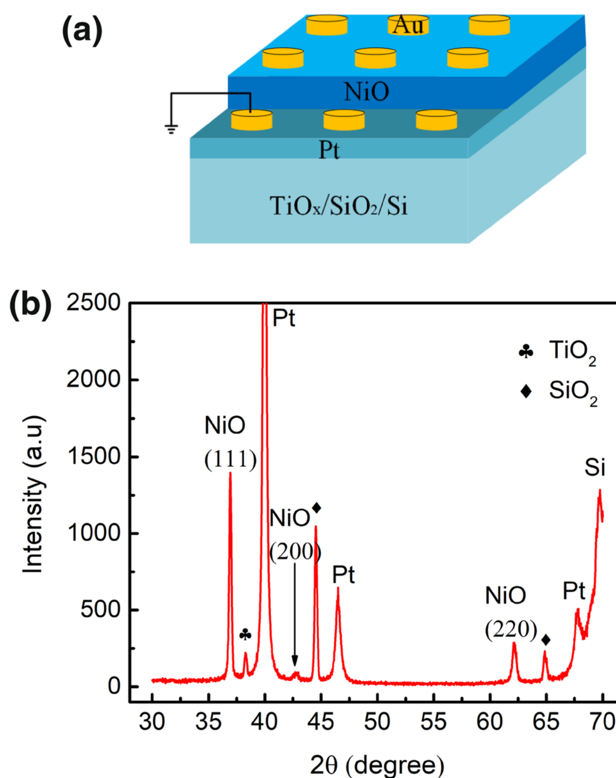

Fig. 1 **a** The device structure and **b** XRD patterns of NiO films

the Si. The strong characteristic diffraction peaks of NiO films at 36.94° relates to the (111) plane, indicating that the polycrystalline NiO films are well formed with an obvious preferred (111) orientation. It is reported by most researches that the (111) planes are polarized [28–31], indicating that most polar charges exist in NiO films.

The Ni 2p and O 1 s XPS spectra of the NiO films are shown in Fig. 2. As shown in Fig. 2, the Ni 2p orbitals have two peaks 872.2 eV and 853.9 eV due to the spin orbit [32], which are assigned to Ni 2p1/2 and Ni 2p3/2 electronic state. A difference value 18.3 eV between the Ni 2p1/2 and Ni 2p3/2 is larger than the theoretical value of 17.3 eV. It may derive from the broad feature of the Ni 2p1/2 peak at 872.2 eV and the shoulder observed at 855.4 eV assigned to Ni^{3+} state [33]. The observed Ni^{3+} state refers to the structure that contains Ni^{2+} ions with holes and not to Ni_2O_3 phase as observed from the XRD results and the O 1 s XPS spectra. The nickel vacancies and Ni^{3+} in NiO crystalline grains can be generated by the following reaction [34, 35]:

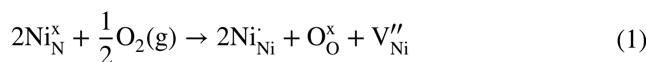

$$2Ni_N^x + \frac{1}{2}O_2(g) \rightarrow 2Ni_{Ni}^{\cdot} + O_O^x + V_{Ni}'' \quad (1)$$

where Ni_{Ni}^x, $Ni_{Ni}^{\cdot}$ and O_O^x represents lattice Ni^{2+}, Ni^{3+} and lattice O^{2-} ions, respectively. The reaction between Ni^{2+} and oxygen produces an ionized nickel vacancy V_{Ni}'' and two Ni^{3+} ions. The created Ni^{3+} ions acting as acceptors impact

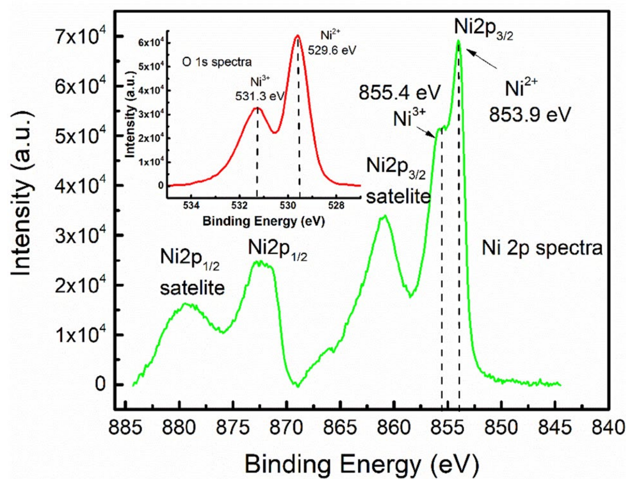

Fig. 2 Ni 2p XPS spectra of the NiO films. The inset is the O 1 s spectra. The peaks at 531.3 eV and 529.6 eV shown in O 1 s spectra relate to Ni^{3+} and Ni^{2+}

the conductive property of the NiO films, indicating that the p-type nonstoichiometric nickel oxide films forms. As shown in O 1 s spectra, the highest intensity peaks found at 529.6 eV is assigned to Ni^{2+} [36]. And the peak at 531.3 eV is assigned to Ni^{3+}, which is an oxygen-containing species and not related to the Ni_2O_3 phase [36]. The results are consistent with the Ni 2p XPS spectra and XRD results.

The I–V characteristic curves with different voltage amplitude are shown in Fig. 3a–d. It can be observed clearly that all the current–voltage curves measured under different voltage amplitude are accord with the exponential relationship, indicating the Schottky junction formed in our device. However, the misalignment current–voltage curves imply the fabricated device presents the resistive switching characteristic. Compared to the resistive switching (RS) characteristic resulting from conducting filament reported in others researches, the I–V behaviors appearing in our device cannot be explained well by the conducting filament due to the exponential relationship between current and voltage. As shown in Fig. 3, the polar RS and NDR are strongly dependent on the voltage polarity. When the applied voltage sweeps from 0 V to positive voltage and returns to 0 V, the electric hysteresis loops are unapparent. However, when applied voltage sweeps at negative voltage region, the electric hysteresis loops are observed obviously compared to sweep at positive voltage region. Nevertheless, when applied voltage sweeps from negative voltage to 0 V, the NDR is obtained which is not observed at positive voltage region and the NDR effect is enhanced with the applied increasing. Meanwhile, the NDR occurs at different negative voltage region (in the vicinity of − 4 V for Fig. 3b, − 6 V for Fig. 3c and − 8 V for Fig. 3d) when different voltage amplitude is applied. Apparently, the origin of NDR resulting from the conducting filament is excluded. The NDR can also be induced by the Joule heating [6, 26]. This mechanism can be excluded because the current is the crucial factor to control the metal–insulator transition resulting in the NDR. It is contrary to the measured data, which the NDR is controlled by voltage.

The XRD results shows the polar charges exists in NiO films which the Schottky barrier height can be affected by [37]. The relationship between the polar charges and the RS is investigated by J.H. Song et al. [38]. According to the thermionic emission theory, the current can be expressed as follow:

$$I = SA^{**}T^2 \exp\left(-\frac{\phi_b}{kT}\right)\left[\exp\left(\frac{qV}{kT}\right) - 1\right] \tag{2}$$

where S is the area of top electrodes, A^{**} represents the effective Richardson constant for thermionic emission, k is the Boltzmann constant, T represents the temperature, q and V are the electron charge and applied voltage, ϕ_b represents the Schottky barrier height, respectively. As depicted in Eq. (2), the current is dependent on the ϕ_b, which results the current varies with the polar charges. However, the NDR is observed only in negative voltage region and the RS at negative voltage region is sensitive to the amplitude of the applied voltage, indicating that the influence of polar charges can be excluded though the polarized (111) planes exists in NiO films. The Pt/NiO or Au/NiO heterointerface may contribute to the I–V characteristic in our device.

To compare our results with those by other researchers [39–42], it has been reported that the Pt/p-NiO/Pt contacts display Ohmic characteristics. This indicates that the non-Ohmic I–V characteristics observed in this work are mainly induced by the Au/NiO heterointerface, not by the Pt/NiO heterointerface. Specifically, these I–V characteristics are strongly dependent on the processes of holes trapped and released by the interface states at the Au/NiO heterointerface. It is similar to the trap-and-release process of electrons reported by Jia et al. in SrTiO3:Nb/ZnO heterojunctions [25]. In order to have a better understanding of this behavior, the schematic diagram of energy band structure and interface states with static bias voltage are depicted in Fig. 4.

As shown in Fig. 4a, when negative voltage is applied initially, a part of holes is trapped by the interface states located at the interface of Au and p-NiO films. Due to the big negative voltage is applied initially, most interface states have trap the holes, the current is increased with the voltage scanning sequentially, indicating that the NDR effect appears. After that, the holes concentration transporting from p-NiO films to Au decreases on account of the smaller energy provided by external electric field to make the holes hurdle the Schottky barrier height,

Fig. 3 The I–V characteristic curves measured at mode I with the amplitude of **a** 2 V, **b** 4 V, **c** 6 V and **d** 8 V

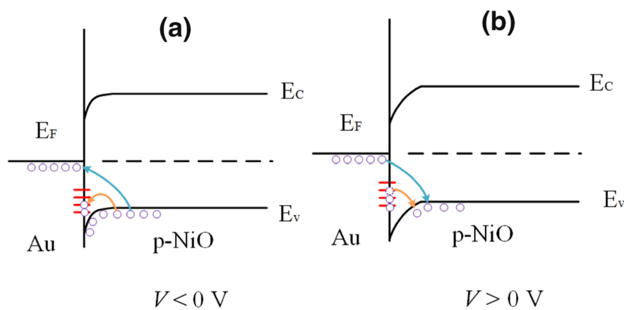

Fig. 4 The schematic diagram of energy band structure and interface state with static bias voltage **a** $V<0$ V and **b** $V>0$ V. The voltage is applied at Au. The orange arrows represent the processes of holes trapped and released. The red stubs represent the interface states located at the interface of Au and p-NiO films

resulting the current decreasing. However, the trapped holes, which contributes to the current, are released from the interface states as shown in Fig. 4b when the positive voltage is applied. At the mode I, when the voltage scans from 0 V to positive voltage, all the trapped holes have inadequate time to be released due to the continuous scanning (The influence of scanning rate on the I–V characteristic curves is discussed later). This delayed of hole release from the 0 V-to-positive scan into the positive-to-0 V scan thus makes the positive-to-0 V current larger than the 0 V-to-positive scan current. When the voltage scans from 0 V to negative voltage, the interface states trap the holes again, which results the current is smaller than scans from negative voltage to 0 V up to all the interface states trap the holes. As a result, the processes of the holes trapped and released has a crucial influence on the RS and NDR. Based on the above analysis, it is easy to understand

the I–V characteristic curves shown in Fig. 3. As shown in Fig. 3a, fewer holes are trapped by interface states due to smaller concentration provided by the smaller negative voltage, resulting the smaller current at positive voltage region compared to the negative voltage region. When a bigger swept voltage with the amplitude 4 V is applied, although more holes are trapped by interface states, most interface states are kept at the initial state. As a result, the released holes at positive voltage region have little contribution to the current. And this also happen to the swept voltage with the amplitude 6 V and 8 V due to the interface states have inadequate time to trap the holes at the mode I.

In order to confirm this, the I–V characteristic curves at the mode II are measured at room temperature and shown in Fig. 5. As Fig. 5 depicts, the scanning rate plays a key role on the RS and NDR. The faster the scanning rate is, the less holes the interface states traps. It is shown in Fig. 5a that the current increase and both the NDR effect and RS characteristic are enhanced with the scanning rate decreasing. When the voltage scans with the scanning rate 0.5 V/0.05 ms, the very distinctly NDR and RS characteristic are obtained. It indicates all the interface states has trapped the hole. Compared to the results shown in Fig. 3, there are three differences: (1) The current at positive voltage region is comparable to the current at negative voltage region. (2) The current swept from 0 V to the positive voltage is bigger than swept from the positive voltage to 0 V shown in Fig. 5. (3) The current peaks, which involves to the released process of holes, can also be observed in positive voltage region when the voltage is swept from 0 to 7 V. The distinction also can be explained by the influence of interface states. At the mode II, the interface states have adequate time to trap the holes and more holes are released when scans from 0 V to the positive voltage, resulting the NDR effect is obvious, the current of positive voltage region are comparable to negative voltage region, the current peaks at positive voltage region and the current swept from 0 V to the positive voltage is bigger than swept from the positive voltage to 0 V. Although all the interface states have trapped the holes at mode II, the influence of the released process of holes is weaken because of the increasing of hole concentration provided by applied voltage with the scanning rate decreasing. As a result, the current peak appearing in positive voltage region disappears with the scanning rate decreasing, which is shown in Fig. 5b.

Based on the previous discussion, the trapped holes by the interface states at the beginning of scanning negative voltage contributes the NDR and polar RS effect. In order to confirm the influence of the interface states again, the sweep mode is replaced by sweeping from 0 to 7 V and return to 0 V from −7 V with different frequency (mode III). The measured data are shown in Fig. 6. Apparently, the I–V characteristic curves are different from the curves discussed

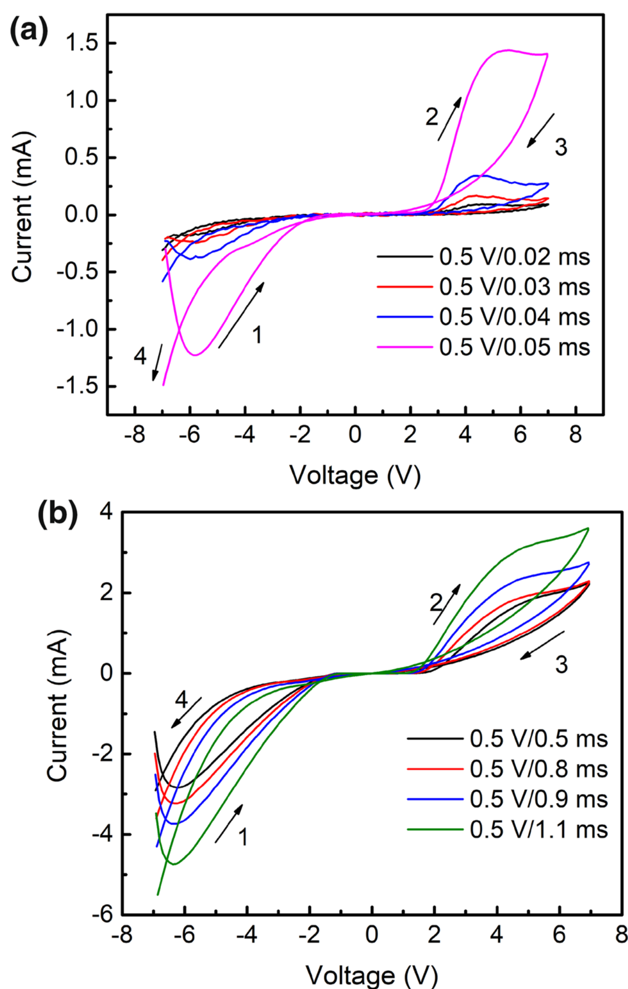

Fig. 5 The I–V characteristic curves measured at mode II

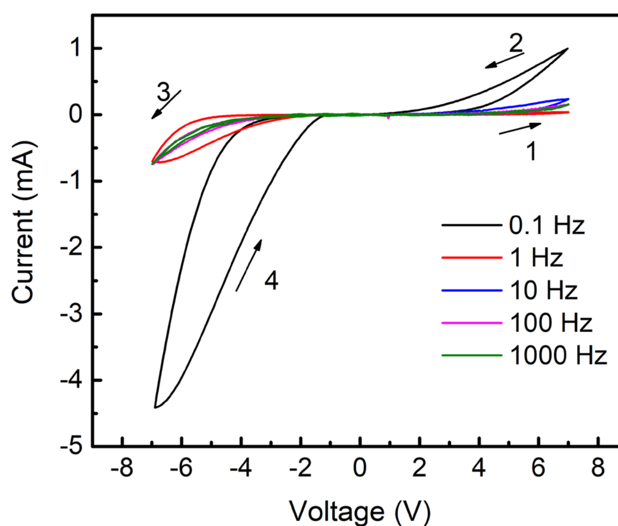

Fig. 6 The I–V characteristic curves as a function of various frequency at mode III

previously. The NDR cannot observed in this sweep mode. At the same time, the current at the positive voltage region is smaller than at negative voltage region. When the voltage scans with the 0 V as starting point, fewer holes are provided by the applied voltage, resulting most interface states are kept the initial state. As a result, the released holes have less contribution to the current and no NDR is found in this sweep mode. It also can be found in Fig. 6 that the current increases with the frequency decreasing. The lower the frequency of the applied voltage, the more holes provided by the applied voltage, which make the current increase.

4 Conclusion

The Au/NiO/Pt structure was fabricated by magnetron sputtering on the $TiO_x/SiO_2/Si$ substrates to investigate the bipolar resistive switching and negative differential resistance in details. The strong characteristic diffraction peaks of NiO films observed at 36.94° relates to the (111) plane, indicating that the polycrystalline NiO films are well formed with an obvious preferred (111) orientation. The shoulder observed at 855.9 eV is assigned to the Ni^{3+} state in Ni 2p and O 1 s spectra XPS spectra, which indicates the p-type nonstoichiometric nickel oxide films forms. The I–V characteristic curves show the bipolar resistive switching accompanied with the distinct negative differential resistance characteristic seriously depend on the scan mode of applied voltage. When the applied voltage scans from negative voltage to positive voltage and return to negative voltage, the negative differential resistance and distinct resistive switching characteristic are obtained. The scanning rate plays an important role on this behavior. The slower the scanning rate is, the more obvious negative differential resistance and resistive switching characteristic can be got. However, when the applied voltage sweeps from 0 V to positive voltage and returned to 0 V from the negative voltage, the negative differential resistance characteristic disappears and the RS characteristic becomes more distinct with the frequency increasing. Those behaviors are highly induced by the interface states located at the interface of Au and p-NiO films by trap and release the holes.

Acknowledgements This work was financially supported by the National Natural Science Foundation of China (Grant Nos. 61671326, 61701338), the National Key Research and Development Program of China (Grant No. 2017YFB0406300).

References

1. F. Pan, S. Gao, C. Chen, C. Song, F. Zeng, Recent progress in resistive random access memories: materials, switching mechanisms, and performance. Mater. Sci. Eng. R Rep. **83**, 1–59 (2014)
2. J. Borghetti, G.S. Snider, P.J. Kuekes, J.J. Yang, D.R. Stewart, R.S. Williams, 'Memristive' switches enable 'stateful' logic operations via material implication. Nature **464**, 873–876 (2010)
3. D.H. Kwon, K.M. Kim, J.H. Jang, J.M. Jeon, M.H. Lee, G.H. Kim, X.S. Li, G.S. Park, B. Lee, S. Han, M. Kim, C.S. Hwang, Atomic structure of conducting nanofilaments in TiO_2 resistive switching memory. Nat. Nanotechnol. **5**, 148 (2010)
4. W.J. Lin, K.J. Zhu, Y.T. Su, H.B. Shi, Y. Meng, H.W. Zhao, In situ observation of conducting filament in NiO memristive devices by electroluminescence. Appl. Phys. Lett. **112**, 202104 (2018)
5. Y. Ahn, H.W. Shin, T.H. Lee, W.H. Kim, J.Y. Son, Effects of a Nb nanopin electrode on the resistive random-access memory switching characteristics of NiO thin films. Nanoscale **10**, 13443–13448 (2018)
6. A.S. Alexandrov, A.M. Bratkovsky, B. Bridle, S.E. Savelev, D.B. Strukov, R.S. Williams, Current-controlled negative differential resistance due to Joule heating in TiO_2. Appl. Phys. Lett. **99**, 202104 (2011)
7. P. Bousoulas, I. Michelakaki, D. Tsoukalas, Influence of Ti top electrode thickness on the resistive switching properties of forming free and self-rectified TiO_{2-x} thin films. Thin Solid Films **571**, 23–31 (2014)
8. S.M. Hua, J.L. Yue, C. Jiang, X.Z. Tang, X.Z. Huang, Z.J. Du, C.Q. Wang, Resistive switching behavior and mechanism in flexible TiO_2@Cf memristor crossbars. Ceram. Int. **45**, 10182–10186 (2019)
9. H.T. Sun, Q. Liu, S.B. Long, H.B. Lv, W. Banerjee, M. Liu, Multilevel unipolar resistive switching with negative differential resistance effect in Ag/SiO_2/Pt device. J. Appl. Phys. **116**, 154509 (2014)
10. R.N. Bhowmik, K.V. Siva, Non-equilibrium character of resistive switching and negative differential resistance in Ga-doped Cr_2O_3 system. J. Magn. Magn. Mater. **457**, 17–29 (2018)
11. A. Kathalingam, H.-S. Kim, S.-D. Kim, H.-M. Park, H.-C. Park, Unipolar resistive switching of solution synthesized ZnO nanorod with self-rectifying and negative differential resistance effects. Mater. Lett. **142**, 238–241 (2015)
12. C. Funck, A. Marchewka, C. Baumer, P.C. Schmidt, P. Müller, R. Dittmann, M. Martin, R. Waser, S. Menzel, A theoretical and experimental view on the temperature dependence of the electronic conduction through a Schottky barrier in a resistively switching $SrTiO_3$-based memory cell. Adv. Electron. Mater. **4**, 1800062 (2018)
13. A. Hao, S. He, N. Qin, R.Q. Chen, D.H. Bao, Ce-doping induced enhancement of resistive switching performance of Pt/$NiFe_2O_4$/Pt memory devices. Ceram. Int. **43**, S481–S487 (2017)
14. K.M. Kim, S.J. Song, G.H. Kim, J.Y. Seok, M.H. Lee, J.H. Yoon, J. Park, C.S. Hwang, Collective motion of conducting filaments in Pt/n-type TiO_2/p-type NiO/Pt stacked resistive switching memory. Adv. Funct. Mater. **21**, 1587–1592 (2011)
15. D.Y. Zhao, S. Qiao, Y.X. Luo, A.T. Chen, P.F. Zhang, P. Zheng, Z. Sun, M.H. Guo, F.K. Chiang, J. Wu, J.L. Luo, J.Q. Li, S. Kokado, Y.Y. Wang, Y.G. Zhao, Magnetoresistance behavior of conducting filaments in resistive-switching NiO with different resistance states. ACS Appl. Mater. Interfaces. **9**, 10835–10846 (2017)
16. D. Kumar, R. Aluguri, U. Chand, T.Y. Tseng, Metal oxide resistive switching memory: materials, properties and switching mechanisms. Ceram. Int. **43**, S547–S556 (2017)
17. X. Kang, J.J. Guo, Y.J. Gao, S.X. Ren, W. Chen, X. Zhao, NiO-based resistive memory devices with highly improved uniformity boosted by ionic liquid pre-treatment. Appl. Surf. Sci. **480**, 57–62 (2019)
18. P. Misra, V.K. Sahu, R.S. Ajimsha, A.K. Das, B. Singh, Studies on resistive switching times in NiO thin films grown by pulsed laser deposition. J. Phys. D **50**, 415106 (2017)

19. Y.X. Luo, D.Y. Zhao, Y.G. Zhao, F.-K. Chiang, P.C. Chen, M.H. Guo, N.N. Luo, X.L. Jiang, P.X. Miao, Y. Sun, A.T. Chen, Z. Lin, J.Q. Li, W.H. Duan, J.W. Cai, Y.Y. Wang, Evolution of Ni nanofilaments and electromagnetic coupling in the resistive switching of NiO. Nanoscale **7**, 642–649 (2015)
20. U. Celano, L. Goux, R. Degraeve, A. Fantini, O. Richard, H. Bender, M. Jurczak, W. Vandervorst, Imaging the three-dimensional conductive channel in filamentary based oxide resistive switching memory. Nano Lett. **15**, 7970–7975 (2015)
21. W.H. Lu, J.X. Xiao, L.-M. Wong, S.J. Wang, K.Y. Zeng, Probing the ionic and electrochemical phenomena during resistive switching of NiO thin films. ACS Appl. Mater. Interfaces. **10**, 8092–8101 (2018)
22. M.Q. Guo, Y.C. Chen, C.Y. Lin, Y.F. Chang, B. Fowler, Q.Q. Li, J. Lee, Y.G. Zhao, Unidirectional threshold resistive switching in Au/NiO/Nb:$SrTiO_3$ devices. Appl. Phys. Lett. **110**, 233504 (2017)
23. R. Mundle, C. Carvajal, A.K. Pradhan, ZnO/Al:ZnO transparent resistive switching devices grown by atomic layer deposition for memristor applications. Langmuir **32**, 4983–4995 (2016)
24. G. Yang, C.H. Jia, Y.H. Chen, X. Chen, W.F. Zhang, Negative differential resistance and resistive switching behaviors in $BaTiO_3$ thin films. J. Appl. Phys. **115**, 204515 (2014)
25. C.H. Jia, X.W. Sun, G.Q. Li, Y.H. Chen, W.F. Zhang, Origin of attendant phenomena of bipolar resistive switching and negative differential resistance in $SrTiO_3$:Nb/ZnO heterojunctions. Appl. Phys. Lett. **104**, 043501 (2014)
26. A.A. Wagh, P.S.A. Kumar, H.L. Bhat, S. Elizabeth, Negative differential resistance in $Gd_{0.5}Sr_{0.5}MnO_3$: a consequence of Joule heating. J. Appl. Phys. **108**, 063703 (2010)
27. Z. Jia, L.K. Wang, N.W. Zhang, T.L. Ren, J.J. Liou, Effects of anode materials on resistive characteristics of NiO thin films. Appl. Phys. Lett. **102**, 042901 (2013)
28. R. Poulain, A. Klein, J. Proost, Electrocatalytic properties of (100)-, (110)-, and (111)-oriented NiO thin films toward the oxygen evolution reaction. J. Phys. Chem. C **122**, 22252–22263 (2018)
29. B. Liu, L. Wang, Y. Ma, Y.K. Yuan, J. Yang, M.Z. Wang, J.F. Liu, X. Zhang, Y. Ren, Q. Du, H. Zhao, C.J. Pei, S.Z. Liu, H.Q. Yang, Enhanced gas–sensing properties and sensing mechanism of the foam structures assembled from NiO nanoflakes with exposed 1 1 1 facets. Appl. Surf. Sci. **470**, 596–696 (2019)
30. J. Goniakowski, F. Finocchi, C. Noguera, Polarity of oxide surfaces and nanostructures. Rep. Prog. Phys. **71**, 016501 (2008)
31. B. Liu, H.Q. Yang, A.H. Wei, H. Zhao, L.C. Ning, C.J. Zhang, S.Z. Liu, Superior photocatalytic activities of NiO octahedrons with loaded AgCl particles and charge separation between polar NiO 111 surfaces. Appl. Catal. B **172–173**, 165–173 (2015)
32. V.R. Reddy, P.R.S. Reddy, I.N. Reddy, C. Choi, Microstructural, electrical and carrier transport properties of Au/NiO/n-GaN heterojunction with a nickel oxide interlayer. RSC Adv. **6**, 105761–105770 (2016)
33. E. Turgut, O. Coban, S. Saritas, S. Tuzemen, M. Yildirimc, E. Gurc, Oxygen partial pressure effects on the RF sputtered p-type NiO hydrogen gas sensors. Appl. Surf. Sci. **435**, 880–885 (2018)
34. T.F. Chen, A.J. Wang, B.Y. Shang, Z.L. Wu, Y.L. Li, Y.S. Wang, Property modulation of NiO films grown by radio frequency magnetron sputtering. J. Alloy. Compd. **643**, 167–173 (2015)
35. P. Yang, L.X. Li, S.H. Yu, H.R. Zheng, W. Peng, The annealing temperature and films thickness effect on the surface morphology, preferential orientation and dielectric property of NiO films. Appl. Surf. Sci. **493**, 396–403 (2019)
36. S. Oswald, W. Bruckner, XPS depth profile analysis of non-stoichiometric NiO films. Surf. Interface Anal. **36**, 17–22 (2004)
37. K.W. Chung, Z. Wang, J.C. Costa, F. Williamson, P.P. Ruden, M.I. Nathan, Barrier height change in GaAs Schottky diodes induced by piezoelectric effect. Appl. Phys. Lett. **59**, 1191–1193 (1991)
38. J.H. Song, Y. Zhang, C. Xu, W.Z. Wu, Z.L. Wang, Polar charges induced electric hysteresis of ZnO nano/microwire for fast data storage. Nano Lett. **11**, 2829–2834 (2011)
39. Y. Lee, H. Kwon, J.-S. Yoon, J.K. Kim, Overcoming ineffective resistance modulation in p-type NiO gas sensor by nanoscale Schottky contacts. Nanotechnology **30**, 115501 (2019)
40. H.-I. Chen, C.-Y. Hsiao, W.-C. Chen, C.-H. Chang, T.-C. Chou, I.-P. Liu, K.-W. Lin, W.-C. Liu, Characteristics of a Pt/NiO thin film-based ammonia gas sensor. Sens. Actuators B **256**, 962–967 (2018)
41. J.-L. Sun, X.C. Zhao, J.-L. Zhu, Metal–insulator transition in Au-NiO-Ni dual Schottky nanojunctions. Nanotechnology **20**, 455203 (2009)
42. N. Brilis, C. Foukaraki, E. Bourithis, D. Tsamskis, A. Giannoudakos, M. Kompitsas, T. Xenidou, A. Boudouvis, Development of NiO-based thin film structures as efficient H_2 gas sensors operating at room temperatures. Thin Solid Films **515**, 8484–8489 (2007)

Publisher's Note Springer Nature remains neutral with regard to jurisdictional claims in published maps and institutional affiliations.